Precise Control of Organic LED Emission Through Optically-Resonant Microcavity Confinement

An Honors Thesis Presented

by

Benjamin Isenhart

to

The Faculty of the University of Vermont

Spring 2019

Defense Date: 2nd May, 2019

Thesis Examination Committee:

Frederic Sansoz, Ph.D., Chairperson

Matthew S. White, Ph.D., Advisor

Madalina Furis, Ph.D.

Abstract

The ability to change the emission spectrum of an LED device has traditionally only been possible through chemical changes to the emissive material or the addition of dopants. Both of these techniques have significant disadvantages due to the limited range of changes possible and the difficulty of precisely controlling these changes. We present a technique of precisely controlling the emission spectrum of a device through device design alone. By placing reflective electrodes on either side of an LED device, we generate an optically resonant microcavity whose properties impact the emission profile of the device. The direct relationship between the cavity thickness and the peak emission wavelength allows for tuning of the peak emission to within the resolution of our ability to deposit films. We additionally explore the impacts of stacking multiple microcavities on top of one another in the emission profile.

Contents

Chapter 1

Introduction

1.1 Organic Light Emitting Diodes

Light emitting diodes (LEDs) have become prevalent in everyday life in applications ranging from screens to the headlights on cars. They have widely replaced the more traditional incandescent bulbs due to increased power efficiency, longevity, and compact size when compared to other luminescent devices. However, many LEDs require hazardous semiconductors such as gallium doped silicon[8]. In order to mitigate this, LEDs based off of organic materials, called OLEDs, have come into fruition, with the first OLEDs being demonstrated by Tang and VanSlyke in 1987. OLEDs are usually comprised of a transparent conductive oxide (TCO) as a transparent electrode, a metal for the non-transparent electrode, and three organic materials. These organic materials are used as a hole transport material, electron transport material, and an emissive material[11]. The emissive material has a band structure suitable for electron and hole recombination and the release of a photon in the visible spectrum. The hole and electron transport materials serve primarily to ensure that all electron-hole recombination occurs in the emissive material. However, current OLED technology is still hindered in their power conversion efficiency, due in part to the low carrier mobilities in organic bulk[11]. Conventionally, the output intensity of an LED could be increased by thicknening the recombination region, providing more recombination sites. With the limited mobility of carriers in organic materials, however, a thicker emission region makes effective charge injection into the recombination sites difficult. A method for mitigating this by stacking multiple OLEDs on top of one another with a shared electrode has been previously demonstrated[5], although this device structure was mainly focused on the applications in stacked pixels for OLED screens.

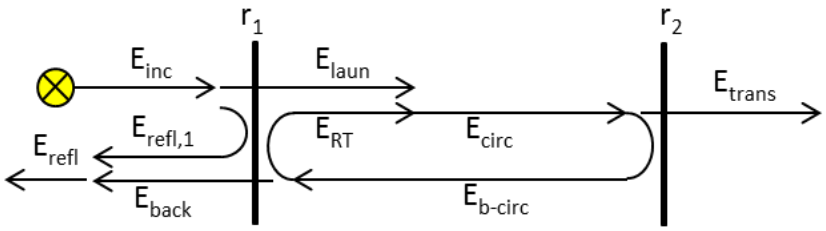

Figure 1.1: Schematic of the Fabry-Pérot etalon. The steady state solutions for wave propogation in the normal mode of the etalon are shown[7].

1.2 Waveguides and the Fabry-Pérot Etalon

In electomagnetism, a waveguide is defined as a surface or set of surfaces made of a conductor such that the electric and magnetic fields within the conductor are restricted to zero. These waveguides provide boundary conditions to Maxwell's equations, such that only specific modes of propogation can occur within the waveguide. These allowed modes are generally called the transverse electric (TE) mode, the transverse magnetic (TM) mode, and in the special case of both TE and TM, the TEM mode[4]. One special form of waveguide, called the Fabry-Pérot etalon, is characterized by two conducting planes with a transparent material in between. Due to the structure of the etalon, certain wavelengths of light resonate in the etalon, while others destructively interfere with their reflections, and are eliminated[7]. In particular, the condition for resonance is that the frequency ν and wavenumber k obey:

$$\nu_q = \frac{qc}{2ln} \text{ and } k_q = \frac{\pi q}{l} \tag{1.1}$$

for the qth resonant mode. Here c is the speed of light in vacuum, l is the geometric length of the etalon, and n is the index of refraction for the material inside[10]. In the case of light propogating normal to the two planes, this condition can be intuitively understood as standing waves that have no amplitude at the metal surfaces. The transmittance of light through the Fabry-Pérot etalon is given by:

$$T(\phi) = \frac{I_{trans}}{I_{inc}} = \frac{(1-R_1)(1-R_2)}{\left(1-\sqrt{R_1R_2}\right)^2 + 4\sqrt{R_1R_2}\sin^2(\phi)} \tag{1.2}$$

where ϕ describes the phase shift between forward and backward propogating waves inside the etalon. In the special case of the resonant mode, $\phi = 0$, so the resonant mode transmittance is given by:

$$T(\nu_q) = \frac{(1-R_1)(1-R_2)}{\left(1-\sqrt{R_1R_2}\right)^2} \tag{1.3}$$

where R_1 and R_2 are the reflectivities of the conductive planes[12].

1.3 Optically Resonant OLED Microcavities

In the traditional Fabry-Pérot etalon, the light source is located outside of the conductor planes, and the spectrum is collected on the opposite side of the conductor planes. In a traditional OLED, an emitting material is located between a conductive electrode and a transparent electrode. By replacing the transparent electrode of an OLED with a partially reflective, partially transmittive film, the two devices can be combined to form Fabry-Pérot etalon with an emissive source inside of it. This device would filter from the broadband emission of the OLED all wavelengths except the resonant modes, forming much narrower emission peaks[6]. In this project, devices of this form were fabricated so that the emission of the OLED device underwent filtration by this optically resonant microcavity and the dependence of the emission spectrum on physical proproperties of the microcavity were explored.

Chapter 2

Experimental Methods

2.1 OLED Materials

An tris-(8-hydroxyquinoline)aluminum (Alq_3) emissive material, along with bathophenanthroline (BPhen) as an electron transport material and N,N-Di(1-naphthyl)-N,N-diphenyl-(1,1-biphenyl)-4,4-diamine (NPB) as a hole transport material, were chosen due to their reported use in a green OLED devices[3, 9]. Silver and molibdinum oxide (Ag/MoO_3) were used for the hole selective electrode, while aluminum and lithium flouride (Al/LiF) were used for the electron selective electrode. The organics were purchased from Sigma-Aldrich and purified through sublimation.

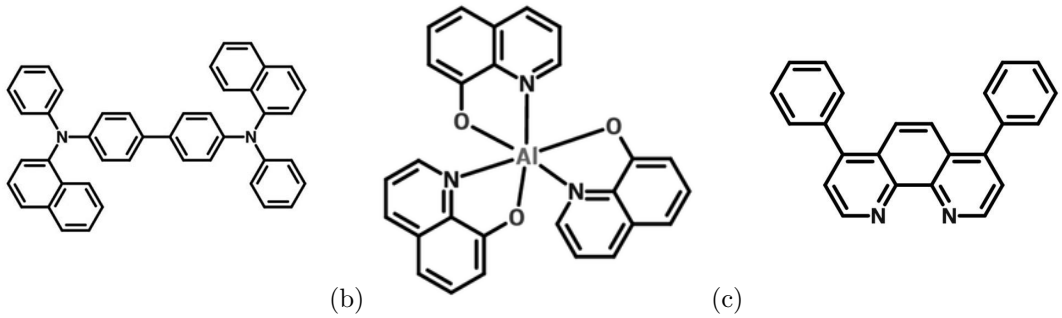

(a) (b) (c)

Figure 2.1: Chemical structures of (a) the NPB hole transport material, (b) the Alq_3 emitter material, and (c) the BPhen electron transport material.

2.2 Device Fabrication

In order to generate optically resonant microcavities, a standard OLED recipe[3, 9] was used with the substitution of a 30nm metal electrode in the place of a transparent electrode. In particular, an oxidized silicon substrate had a 100nm bottom electrode of silver, followed by 1nm of molibdinum oxide, $x$nm of NPB, 20 (single cavity devices) or 26nm (multi-cavity devices) of Alq_3, $x$nm of BPhen, 1nm of lithium flouride, and 30nm of aluminum deposited onto it through sequential thermal evaporation. For multi-cavity devices, this same structure was replicated in the following cavity, but inverted, as shown in Figure 2.2. The thickness x of the NPB and BPhen layers was modified to generate whatever cavity thickness was desired. In all multi-cavity devices transport layer thicknesses of $x = 40$nm were used. All depositions were performed under a pressure of 10^{-7}torr and vacuum was not broken during processing.

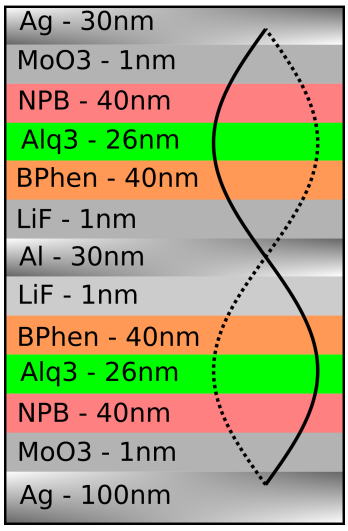

Figure 2.2: Schematic of a two-cavity device and the $\lambda/2$ resonant mode.

2.3 Emission Spectroscopy

Devices were stored and tested in a nitrogen glovebox with < 0.01ppm O_2 and < 0.05ppm H_2O to avoid degradation of devices. Emission spectra were collected using an OceanOptics (NAME?) spectrometer with a fiberoptic passthrough to the glovebox. The emission of the devices was passed through an iris to minimize the collection angle, then reflected off of a parabolic mirror to focus the emission into the fiber. Devices were mounted on a rotating stage and emission spectra were collected at 2.5 degree intervals from 0 to 90 degrees.

Chapter 3

Results

3.1 Single Cavity Devices

In all single cavity devices, a 100nm bottom electrode was used with a 30nm top electrode to produce a resonant cavity of the desired size. The thickness of the organics was changed in order to maintain a 20nm Alq_3 layer between the contact layers. In all devices except those described in section 3.1.3, a silver electrode with a MoO_3 cap was used as the bottom electrode and an aluminum electrode with a LiF cap was used for the top.

3.1.1 Peak Emission Wavelength

An analysis of the peak wavelength of emission for each cavity thickness reveals a very strong correlation. In particular, a linear relationship is observed between the peak wavelength and the resonance cavity thickness, as shown in Figure 3.2. This is logical as the wavelength of a resonant mode should be proportional to the width of the resonance cavity, with the constant of proportionality being the index of refraction for light in the organic materials. We do see some variation from the linear model, which is to be expected the overall index of refraction in the cavity is not a constant across devices. Specifically,

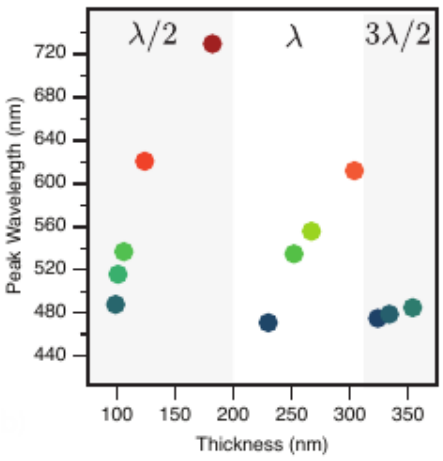

Figure 3.2: Peak emission wavelength as a function of thickness for various single cavity devices.

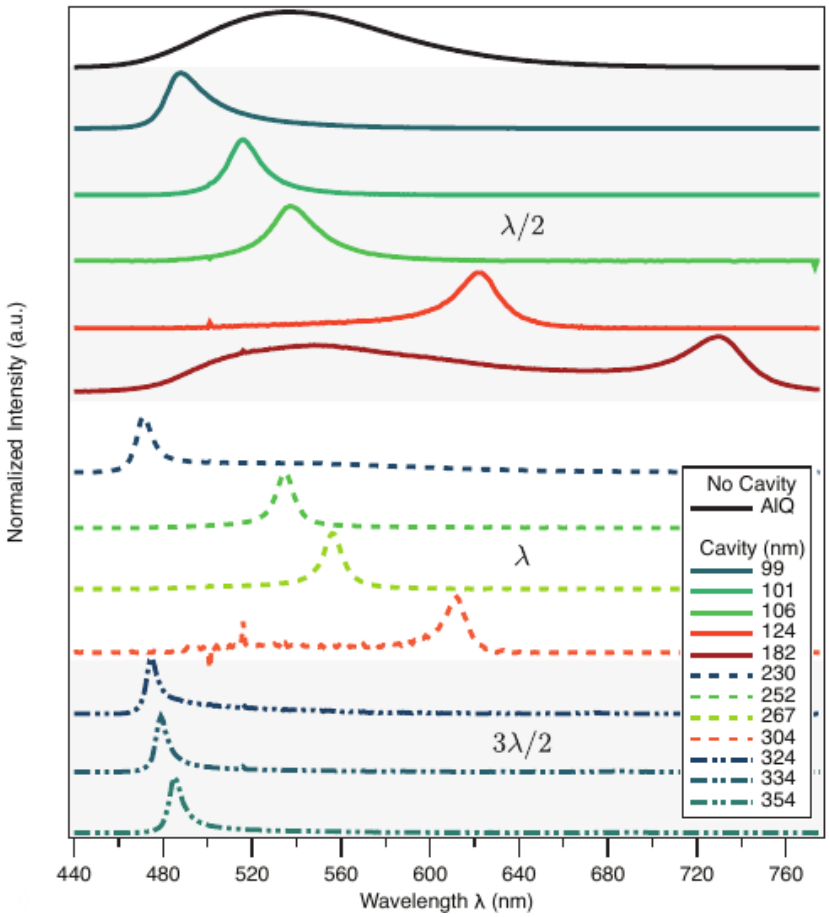

Figure 3.1: Emission spectra of single cavity devices of various cavity thicknesses, along with the natural emission spectrum of the Alq_3 emitter. As cavity thickness increases, the emission peak redshifts, until it shifts to the next resonant mode, returning to a blue color. Following each shift to the next resonant mode, the bandwidth of the emission narrows. The 182nm device shows a strong broadband emission along with the resonant mode. That is because the natural emission at the wavelength of the resonant mode is extremely weak, so the broadband leakage out of the cavity is on the same order as the resonant emission.

by not keeping the ratio of each organics layer the same, we inadvertantly modified the index of refraction slightly, leading to small variations from the linear model.

The linear model, however, is only valid for the regime of a single resonant mode. We see a break in the linearity of peak emission wavelength and cavity thicknesses at the points of transition from a half-integer resonance to the next. We have measured the transition from $\lambda/2$ to λ and from λ to $3\lambda/2$ at approximately 200nm and 310nm, respectively. This is as expected, as the resonant wavelength doubles when shifting from one half-integer mode to the next. We also notice that when the linear relationship picks up again on the other side of a transition to the next mode, the slope is decreased, indicating that the constant of proportionality discussed above is not just dependent on the index of refraction, but also which resonant mode is being described.

3.1.2 Band Narrowing

Analysis of the band width of the emission can be analyzed through the use of the quality factor. The quality factor is defined as:

$$Q = \frac{\nu_0}{\Delta\nu_{1/2}} \tag{3.1}$$

where ν_0 is the resonant frequency and $\Delta\nu_{1/2}$ represents the full width at half max of the emission spectrum in Fourier space[14]. By solving for the steady state solutions of the Fabry-Pérot etalon, we find that $\Delta\nu_{1/2}$ is given by:

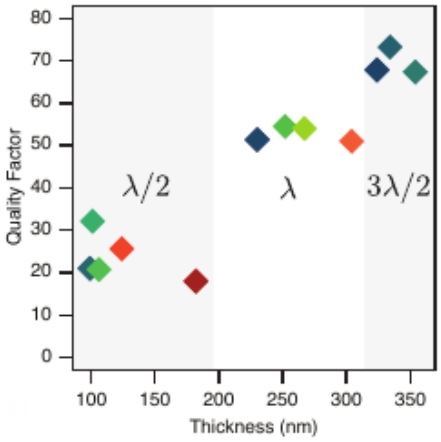

Figure 3.3: Quality factor as a function of cavity thickness for various single cavity devices.

$$\Delta\nu_{1/2} = \frac{c}{2nd}\frac{1-\sqrt{R_1R_2}}{\pi(R_1R_2)^{1/4}} \tag{3.2}$$

where c is the speed of light in the organics, n is integer describing the mode, and d is the cavity thickness[14]. Then, taking the resonant frequency ν_0 to be the frequency of the peak intensity light:

$$\nu_0 = \frac{c}{\lambda_0} \tag{3.3}$$

We can obtain an expression for the quality factor of the device:

$$Q = \frac{\nu_0}{\Delta\nu_{1/2}} = \frac{c}{\lambda_0}\frac{2nd}{c}\frac{1-\sqrt{R_1R_2}}{\pi(R_1R_2)^{1/4}} = \frac{2nd}{\lambda_0}\frac{1-\sqrt{R_1R_2}}{\pi(R_1R_2)^{1/4}} \tag{3.4}$$

Now, by introducing q to be the number of half wavelengths in the cavity:

$$q = \frac{2nd}{\lambda_0} \tag{3.5}$$

We see that the quality factor depends only on q and the reflectivities of the metal electrodes:

$$Q = q\left\{\frac{1-\sqrt{R_1R_2}}{\pi(R_1R_2)^{1/4}}\right\} \tag{3.6}$$

Therefore, the steady state solutions of the Fabry-Pérot etalon predict the quality factor to be a step function in q, which is confirmed by the data displayed in Figure 3.3

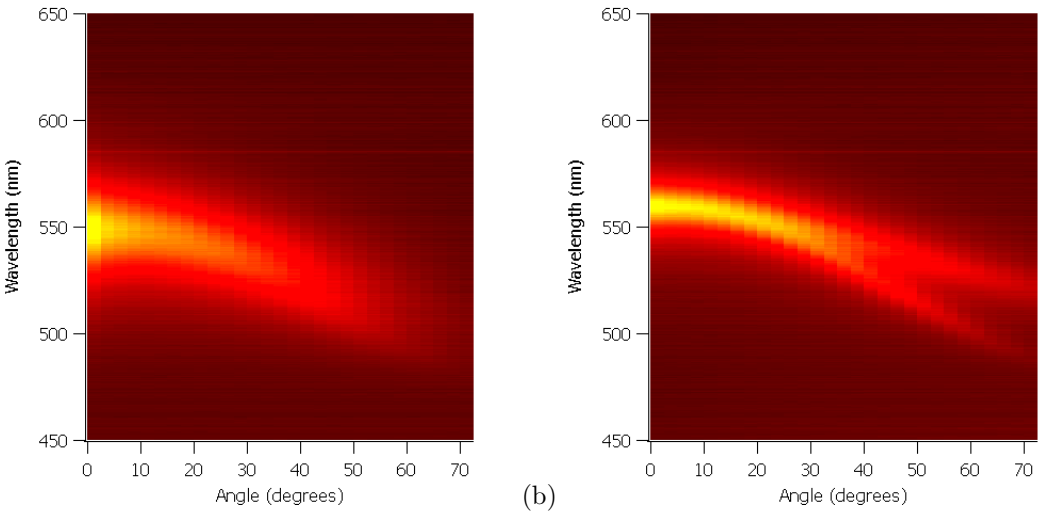

Figure 3.4: Angular resolved emission profiles of single cavity devices topped with a silver electrode (a), and with an aluminum electrode (b). The aluminum topped device shows a much narrower emission peak than the silver topped device due to differences in optical properties of the metals.

3.1.3 Effect of Top Electrode Material

As fabrication of the multi-cavity devices requires both regular and inverted devices, two devices were fabricated in identical conditions except that they were inverted with respect to each other. Each has a 100nm bottom electrode, 1nm capping layer, followed by a 40/26/40 set of organics layers, with a 1nm cap and 30nm top electrode, as was done with the multicavity devices. In comparing the emission spectra of the two devices, we see a massive difference. In particular, the aluminum topped device has a much narrower emission spectrum than the sliver topped device. The contrast in emission spectra is due to the differing optical properties of silver and aluminum. While both have similar transmittivities, aluminum absorbs a significant amount more than silver, and reflects significantly less[13]. In the aluminum topped device, almost all light that travels towards the bottom electrode is reflected by the 100nm silver electrode, strongly pinning that light to the resonant wavelength, which can then be partially transmitted through the top aluminum electrode. In the case of the silver topped device, however, the lower reflectivity on the bottom electrode gives a weaker resonant mode to be transmitted through the top electrode.

3.2 Multi-cavity Devices

In all multi-cavity devices, a 100nm silver bottom electrode was used, with all subsequent electrodes at a thickness of 30nm. The cavities were created using a 26nm film of the Alq_3 emitter with 40nm contact layers on either side. This generates 126nm cavities for all multi-cavity devices.

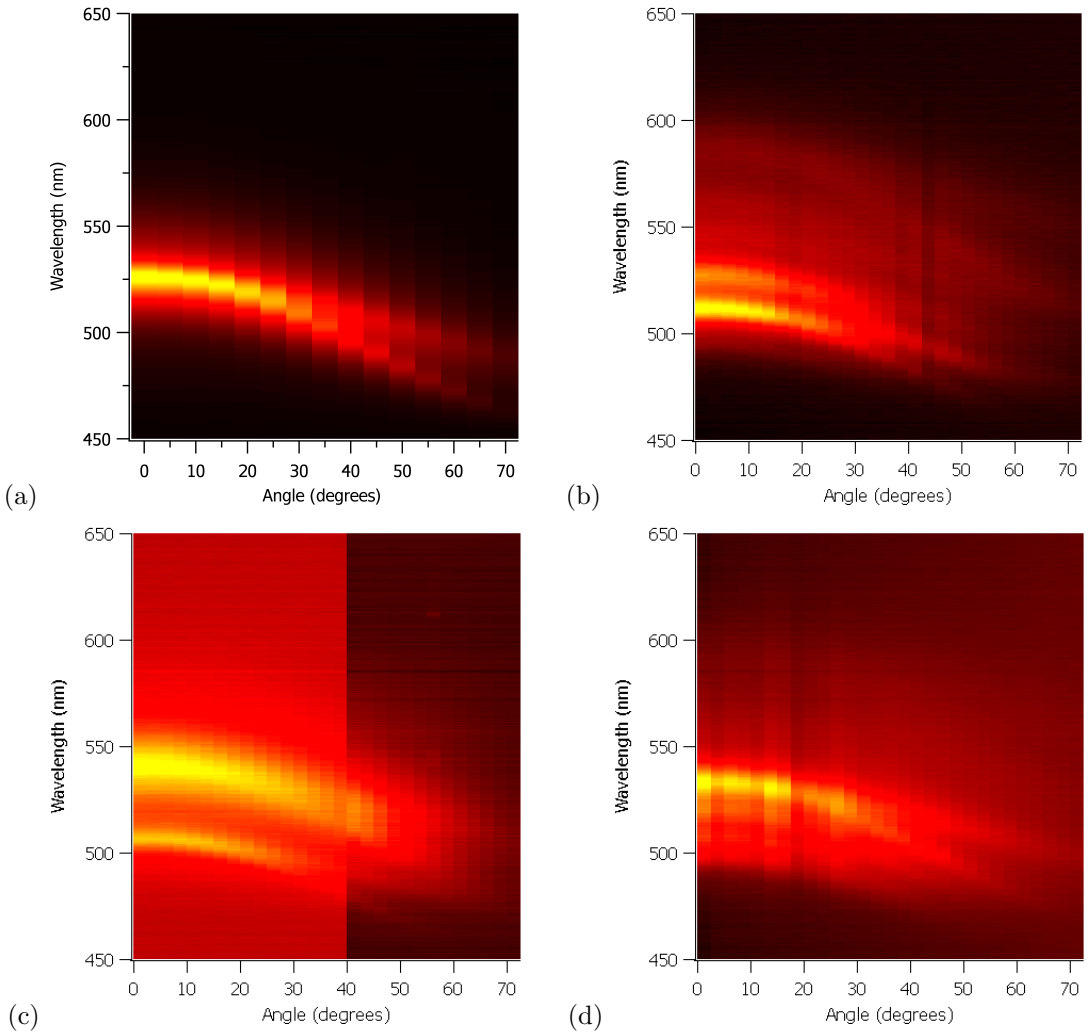

Figure 3.5: Angular resolved emission profiles of devices with two (a), three (b), four (c), and five (d) cavities. The modal splitting of TE and TM modes can be seen along with the increase in emission modes at higher numbers of resonant cavities. The change in background intensity in the four cavity device (c) is due to a change in the iris size during data collection to maintain a strong signal.

3.2.1 Behavior at Large Angles

In the angular resolved emission spectroscopy, we see that the emission profile of the resonance cavities are highly dependent on the viewing angle. The peak emission blueshifts parabolically with increasing angle, and the emission splits into two distinctive peaks that separate as the angle increases. This is as would be predicted by the theory of wave propagation in a Fabry-Pérot etalon[8]. The modal splitting is the separation of the transverse electric (TE) and transverse magnetic (TM) modes splitting off from the superposition of them at $\theta = 0$, called the transverse electric and magnetic (TEM) mode.

3.2.2 Number of Resonant Modes

We additinally see that a more complex modal structure can be generated with multi-cavity devices, even in forward emission. We see the first transition from one to two forward emission peaks in the transition from N=2 to N=3. The N=3 device has a narrow and intense emission peak at approximately 510nm with a slightly wider and weaker peak around 525nm. In the N=4 device, we also see two forward emission peaks, but the one around 510nm is significantly narrower and less intense with a broader, more intense peak occuring around 540nm. In the transition from N=4 to N=5, we see almost perfect preservation of the modal structure of N=4, with an additional peak superimposed between the two existing peaks. Although the cause of these additional peaks is not abundantly clear, the existence of two modes, one narrower than the other is logical. For example, in the N=4 device, the narrow peak could be generated by a resonant mode streching across the bottom three devices, while the broad peak is generated from resonances off of both the inner and outer interfaces of the top metal electrode. However, more experimentation would be necessary to confirm this theory.

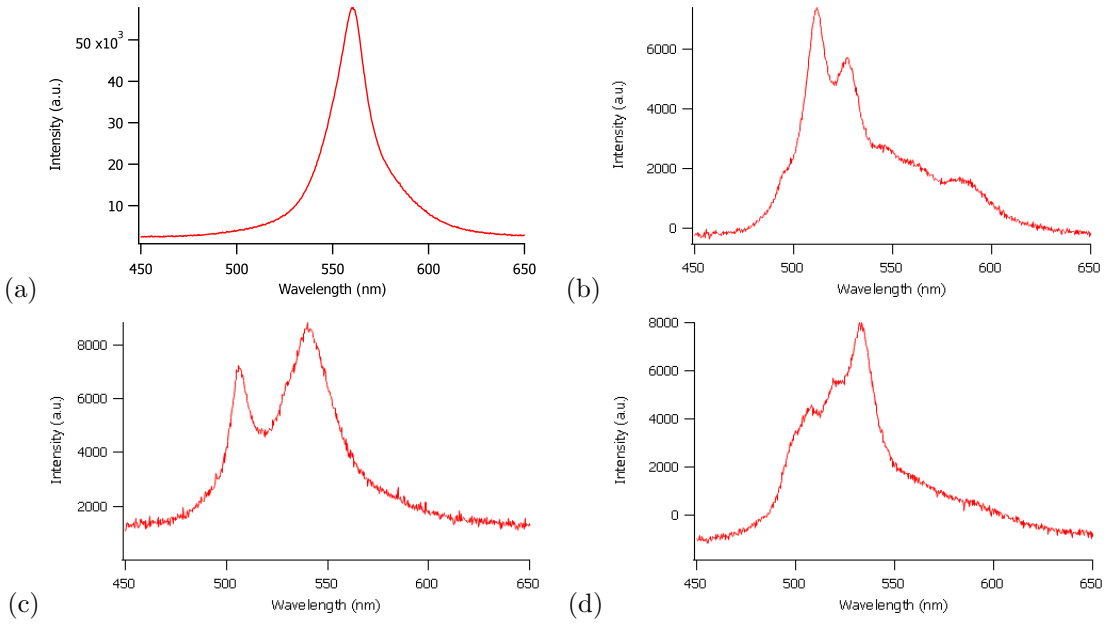

Figure 3.6: Forward emission spectra of devices with two (a), three (b), four (c), and five (d) cavities. The transition from two to three cavities shows the introduction of an additional resonance mode, as does the transition from the four to the five cavity device. Additionally, the width of resonant peaks shrinks as more cavities are introduced.

Number of Cavities	Peak Wavelength	Bandwidth
2	560nm	19.77nm
3	512nm	15.96nm
	527nm	17.25nm
4	507nm	15.25nm
	541nm	15.91nm
5	533nm	11.64nm

Figure 3.7: Bandwidths of emission peaks in multi-cavity devices. Bandwidth is seen to shrink in all modes with the addition of another resonance cavity. Although three peaks exist in the N=5 device, only one peak is isolated enough to fit a reasonable Lorentzian to it.

3.2.3 Bandwidth of Resonant Modes

By fitting with Lorentzian functions, the full width at half max (FWHM) can be found for each emission peak. By analyzing the FWHM for the emission peaks, we find a definite correlation that the emission bands narrow significantly as the number of cavities increases. This is expected for modes that form a resonant standing wave across several cavities for reasons similar to those presented in Section 3.1.2. As the number of cavities increases, the uncertainty in the position of a photon in the resonant mode increases, allowing for a more precise determination of its momentum, giving a narrower emission peak.

Chapter 4

Conclusion

In this project, we have demonstrated a technique for controlling the bandwidth and peak emission wavelength of an OLED device, as well as generating more complex emission profiles. This technique utilizes device design alone, rather than chemical changes to the emitter materials. The relationships of both peak emission wavelength and bandwith with the thickness of the cavity allows for the ability to design and fabricate a device to match any desired single peak emission profile, provided an emissive material with a sufficiently wide broadband emission spectrum is used. However, the same level of control can not yet be exerted over the complex emission spectra of multi-cavity devices.

In the future, we hope to study the multicavity emission in more detail. In particular, a collection of emission spectra from multi-cavity devices with a different cavity thickness could contribute to a better understanding of the relationship of the emission peaks and polarization analysis of the emission spectra of multi-cavity devices could lead to a stronger understanding of the modal structure of these devices. Additionally, more exploration into the band narrowing of multicavity devices could lead to the ability to make extremely narrow emission devices.

Optically resonant microcavity confined OLEDs could see many applications, such as in low cost screens or optics. In the fabrication of screens, these devices could replace the traditional three emitter materials with a single emitter material deposited over a patterned substrate to generate pixels with different colors while only requiring a single emitter deposition. The ability to generate narrow bandwidth light from cheap organic materials could also be beneficial in optical applications. If the bandwidth continues to narrow with more cavities, it is also possible that a many-cavity stacked device could reach the lasing threshold through electrical pumping[1, 2].

Chapter 5

References

[1] M. A. Baldo, R. J. Holmes, and S. R. Forrest. "Prospects for electrically pumped organic lasers". In: *Physical Review B* 66.3 (July 2002). DOI: 10.1103/physrevb.66.035321. URL: https://doi.org/10.1103/physrevb.66.035321.

[2] V. Bulovi. "Transform-Limited, Narrow-Linewidth Lasing Action in Organic Semiconductor Microcavities". In: *Science* 279.5350 (Jan. 1998), pp. 553–555. DOI: 10.1126/science.279.5350.553. URL: https://doi.org/10.1126/science.279.5350.553.

[3] Min Cai et al. "Indium-tin-oxide-free tris(8-hydroxyquinoline) Al organic light-emitting diodes with 80% enhanced power efficiency". In: *Applied Physics Letters* 99.15 (Oct. 2011), p. 153303. DOI: 10.1063/1.3634210. URL: https://doi.org/10.1063/1.3634210.

[4] D.J. Griffiths. *Introduction to Electrodynamics*. Prentice Hall, 1999. ISBN: 9780138053260. URL: https://books.google.com/books?id=M8XvAAAAMAAJ.

[5] G. Gu et al. "Transparent stacked organic light emitting devices. I. Design principles and transparent compound electrodes". In: *Journal of Applied Physics* 86.8 (Oct. 1999), pp. 4067–4075. DOI: 10.1063/1.371331. URL: https://doi.org/10.1063/1.371331.

[6] Emily S. Hellerich et al. "Deep blue/ultraviolet microcavity OLEDs based on solution-processed PVK:CBP blends". In: *Organic Electronics* 24 (Sept. 2015), pp. 246–253. DOI: 10.1016/j.orgel.2015.05.041. URL: https://doi.org/10.1016/j.orgel.2015.05.041.

[7] Nur Ismail et al. "Fabry-Pérot resonator: spectral line shapes, generic and related Airy distributions, linewidths, finesses, and performance at low or frequency-dependent reflectivity". In: *Optics Express* 24.15 (July 2016), p. 16366. DOI: 10.1364/oe.24.016366. URL: https://doi.org/10.1364/oe.24.016366.

[8] Seong-Rin Lim et al. "Potential Environmental Impacts of Light-Emitting Diodes (LEDs): Metallic Resources, Toxicity, and Hazardous Waste Classification". In: *Environmental Science & Technology* 45.1 (Jan. 2011), pp. 320–327. DOI: 10.1021/es101052q. URL: https://doi.org/10.1021/es101052q.

[9] Toshinori Matsushima, Guang-He Jin, and Hideyuki Murata. "Marked improvement in electroluminescence characteristics of organic light-emitting diodes using an ultrathin hole-injection layer of molybdenum oxide". In: *Journal of Applied Physics* 104.5 (Sept. 2008), p. 054501. DOI: 10.1063/1.2974089. URL: https://doi.org/10.1063/1.2974089.

[10] Markus Pollnau. "Counter-propagating modes in a Fabry–Perot-type resonator". In: *Optics Letters* 43.20 (Oct. 2018), p. 5033. DOI: 10.1364/ol.43.005033. URL: https://doi.org/10.1364/ol.43.005033.

[11] Joseph Shinar and Ruth Shinar. "Organic light-emitting devices (OLEDs) and OLED-based chemical and biological sensors: an overview". In: *Journal of Physics D: Applied Physics* 41.13 (June 2008), p. 133001. DOI: 10.1088/0022-3727/41/13/133001. URL: https://doi.org/10.1088/0022-3727/41/13/133001.

[12] A.E. Siegman. *Lasers*. University Science Books, 1986. ISBN: 9780935702118. URL: https://books.google.com/books?id=1BZVwUZLTkAC.

[13] P. N. Stavrinou et al. "Angular spectrum of visible resonant cavity light-emitting diodes". In: *Journal of Applied Physics* 86.6 (Sept. 1999), pp. 3475–3477. DOI: 10.1063/1.371233. URL: https://doi.org/10.1063/1.371233.

[14] Joseph Thomas Verdeyen. *Laser Electronics*. Prentice Hall series in solid state physical electronics. Prentice Hall, 1995. ISBN: 9780137066667. URL: https://books.google.com/books?id=WvFRAAAAMAAJ.

Appendix A

Component Spectra of Angular Resolved Graphs

Single Cavity Aluminum Topped Device

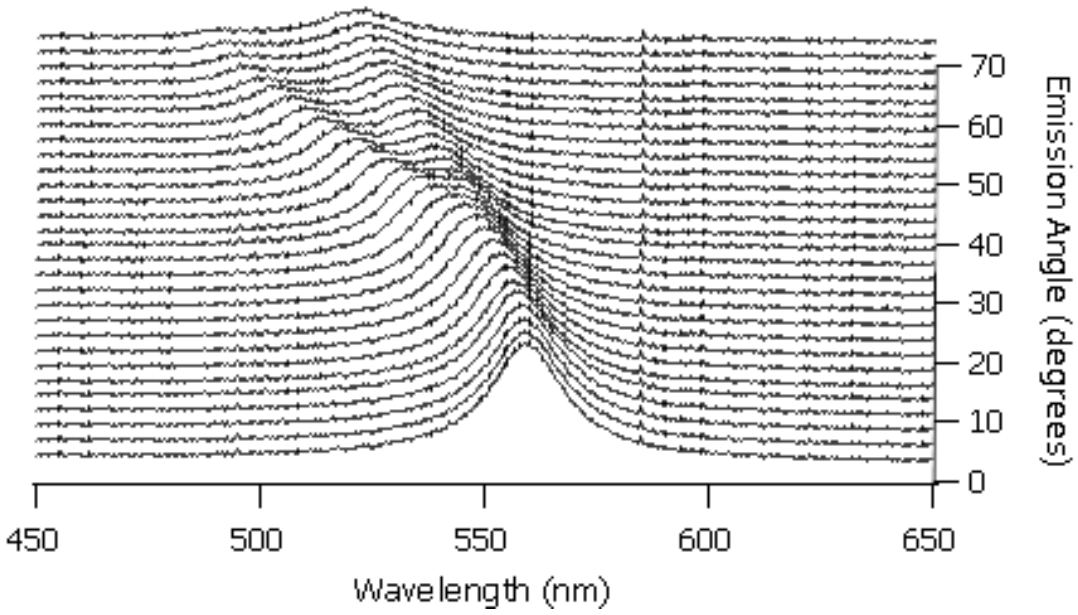

Single Cavity Silver Topped Device

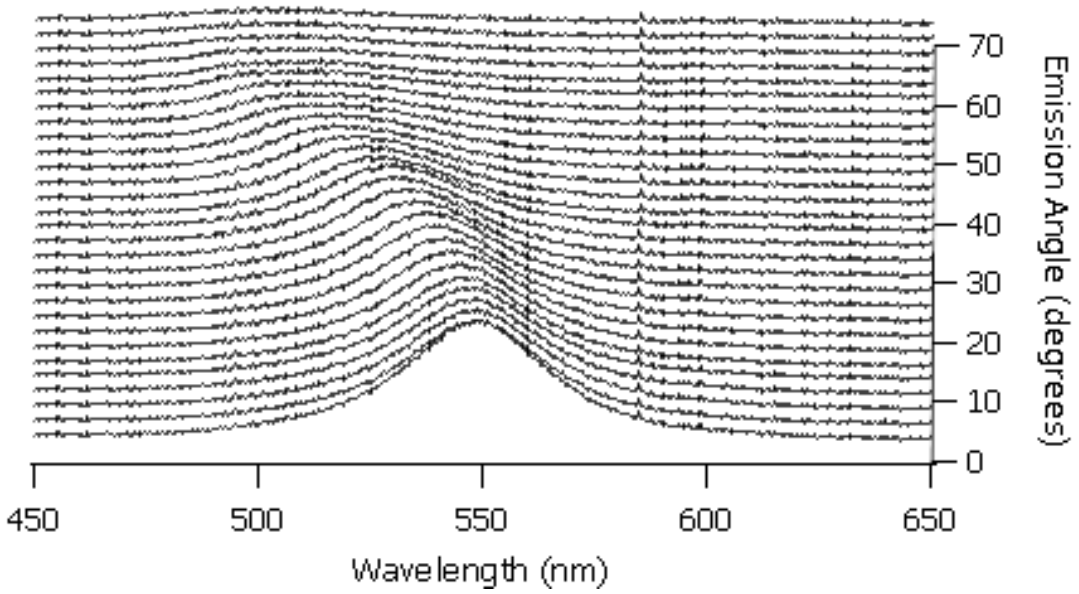

Two Cavity Device

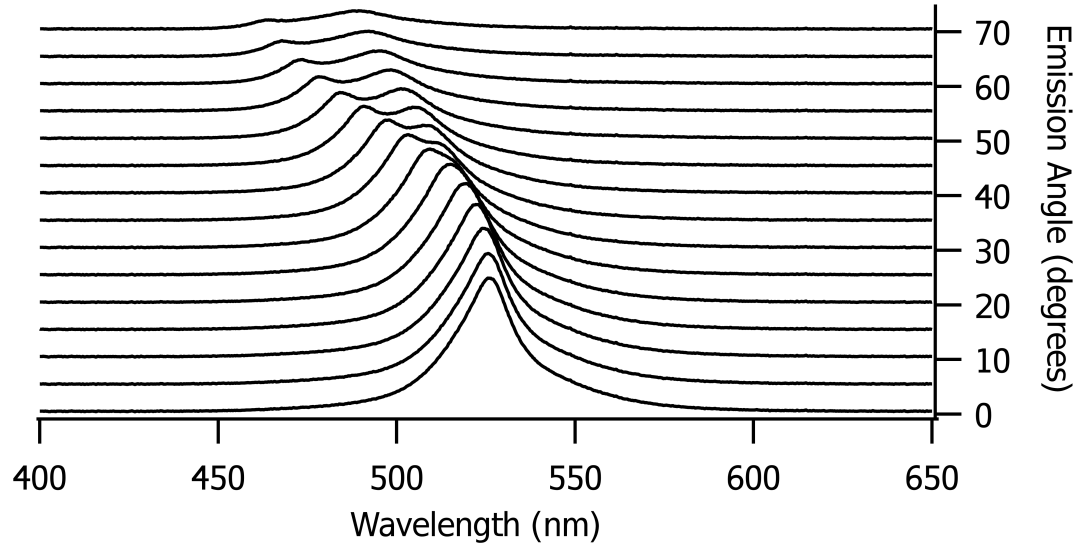

Three Cavity Device

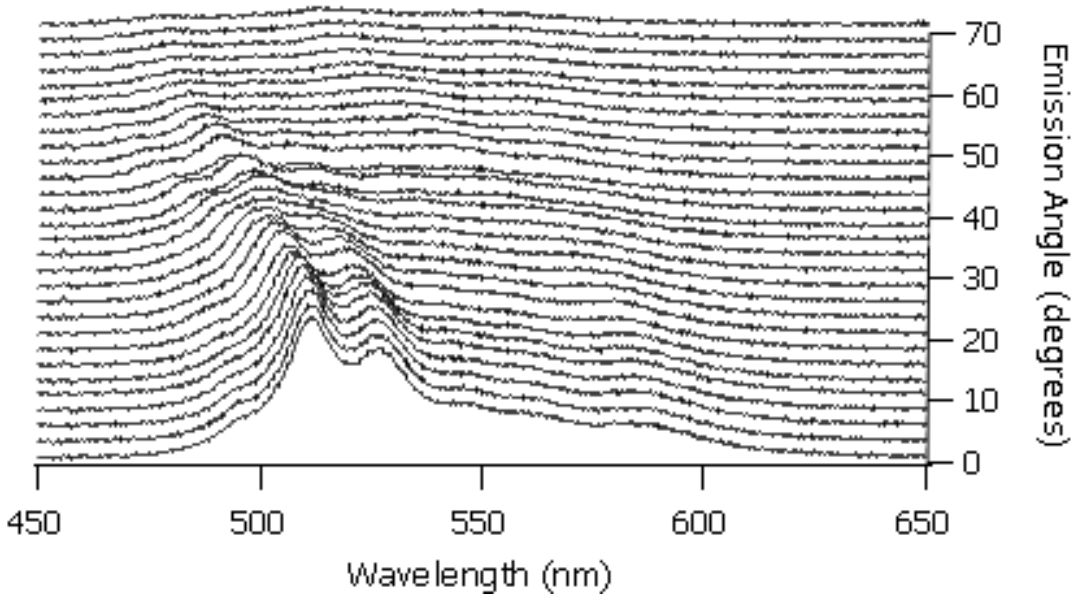

Four Cavity Device

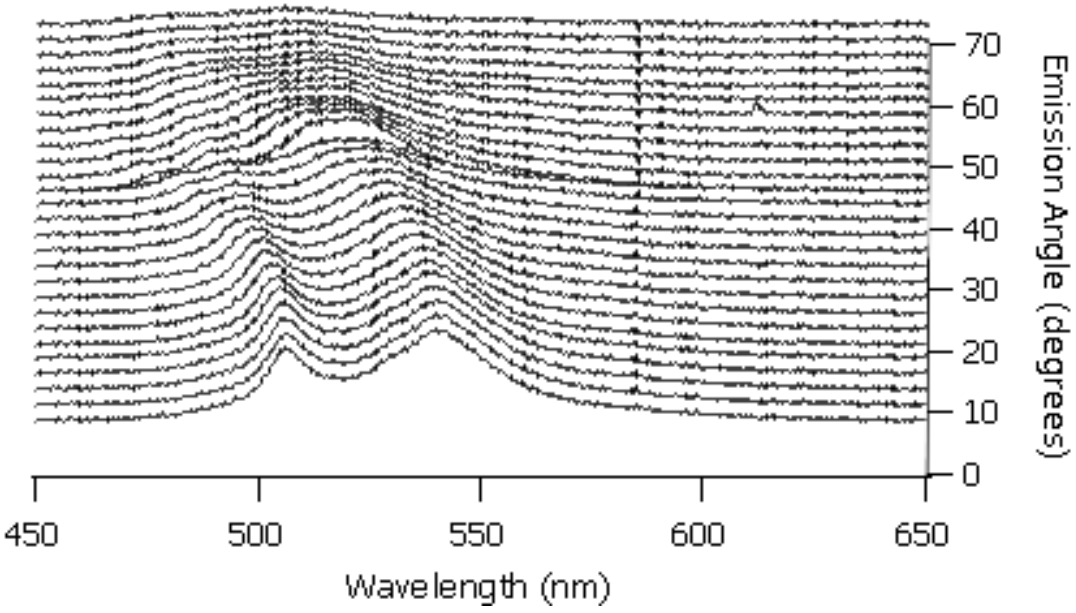

Five Cavity Device